J Sci Comput
DOI 10.1007/s10915-010-9430-x

Shallow Water Flows in Channels

Gerardo Hernández-Dueñas · Smadar Karni

Received: 16 November 2009 / Revised: 2 August 2010 / Accepted: 19 October 2010

Abstract We consider the shallow water equations for flows through channels with arbitrary cross section. The system forms a hyperbolic set of balance laws. Exact steady-state solutions are available and are controlled by the relation between the bottom topography and the channel geometry. We use a Roe-type upwind scheme for the system. Considerations of conservation, near steady-state accuracy, velocity regularization and positivity near dry states are discussed. Numerical solutions are presented illustrating the merits of the scheme for a variety of flows and demonstrating the effect of the interplay between the topography and the geometry on the solution.

Keywords Hyperbolic conservation laws · Balance laws · Upwind schemes · Steady-state solutions

1 Introduction

The shallow water equations model a variety of atmospheric and geophysical flows. They may be derived from the Euler equations by cross sectional averaging, and describe flows that are nearly horizontal. They form a set of nonlinear hyperbolic conservation laws with geometric source terms representing the topography and geometry constraining the flow. Delicate balance between the flux gradient and the geometric source terms give rise to a range of interesting flows including a variety of non-trivial equilibrium solutions. This paper is concerned with shallow water flows through channels of variable cross sectional area, where the interplay between the bottom topography and the contraction of the channel affects and controls the resulting solution. While the model is formulated for channels with a

Work supported in part by NSF, award number DMS 0609766, and by Conacyt #160147.

G. Hernández-Dueñas · S. Karni (✉)
Department of Mathematics, University of Michigan, Ann Arbor, MI 48109-1043, USA
e-mail: karni@umich.edu

G. Hernández-Dueñas
e-mail: gerahdez@umich.edu

Published online: 09 November 2010

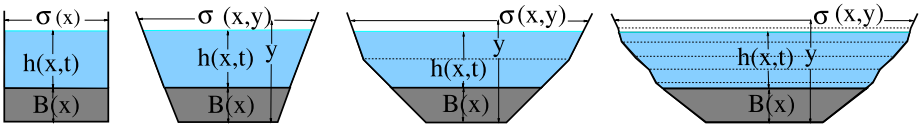

Fig. 1 Schematic of channel cross section

general cross section, it is convenient to think of the channel walls as being approximated by piecewise linear segments, and the cross section being approximated by piecewise trapezoids, see Fig. 1.

Recent years have seen a rapidly growing interest in the development of numerical methods for shallow water systems in various numerical frameworks [1, 2, 10, 12, 14, 15, 17–20, 22, 23], see also the recent book [4] and references cited therein. Most relevant for the present work are papers involving shallow water flows in variable geometry, including [9, 13, 24] where an upwind scheme for the single layer shallow water is derived and generalized to rectangular channel flows, and [6] where the Q-scheme [5] is used to solve the two layer shallow water system, the scheme in [8, 25] based on central WENO reconstruction and [2] using a central-upwind scheme [15].

The paper is organized as follows: In Sect. 2, the model and its properties are described, Sect. 3 discusses the numerical method, and Sect. 4 presents numerical results. The paper has two Appendices: Appendix A discusses the structure of steady-state solutions and the role of boundary conditions, and Appendix B derives the numerical scheme and establishes its properties.

2 The Model

The shallow water equations for flows through channels with variable cross section is given by

$$\begin{pmatrix} A \\ Au \end{pmatrix}_t + \begin{pmatrix} Au \\ Au^2 + I_1 \end{pmatrix}_x = \begin{pmatrix} 0 \\ I_2 - g\sigma_B(x) h B_x \end{pmatrix} \tag{1}$$

where h denotes the depth of the layer, u the velocity, $B(x)$ the bottom topography, $\sigma(x, y)$ the channel geometry, $A = \int_B^{B+h} \sigma(x, y) dy$ is the cross-sectional wet area, $Au = Q$ is the flow rate or discharge, $\sigma_B(x) = \sigma(x, B(x))$ the bottom channel width, and g the gravitational constant. We further use $w = h + B$ to denote the total surface height, $I_1 = g \int_B^w (w - y)\sigma(x, y) dy = Ap$, where p denotes the cross-sectional average of the hydrostatic pressure, and $I_2 = g \int_B^w (w - y)\sigma_x(x, y)\, dy$ (see Fig. 1). Written in quasilinear form, the system is given by

$$\begin{pmatrix} A \\ Au \end{pmatrix}_t + \begin{pmatrix} 0 & 1 \\ c^2 - u^2 & 2u \end{pmatrix} \begin{pmatrix} A \\ Au \end{pmatrix}_x = \begin{pmatrix} 0 \\ c^2 (hI_3 - \sigma_B B_x) \end{pmatrix} \tag{2}$$

where $I_3 = \frac{1}{h} \int_B^w \sigma_x(x, y)\, dy$ is the averaged width variation, and $c^2 = gA/\sigma_T$, where $\sigma_T = \sigma(x, h + B)$ is the width of the channel at the top surface. Notice that c^2 reduces to the familiar expression $c^2 = gh$ for rectangular channels. The system is hyperbolic, with eigenvectors and eigenvalues

$$R = \begin{pmatrix} 1 & 1 \\ u - c & u + c \end{pmatrix}, \qquad \Lambda = \begin{pmatrix} u - c & 0 \\ 0 & u + c \end{pmatrix}, \tag{3}$$

and is characterized by the nondimensional Froude number F, where $F^2 = \frac{u^2}{c^2}$. The flow is described as subcritical for $F^2 < 1$ and supercritical for $F^2 > 1$.

The system is endowed with an entropy function

$$\mathcal{E} = AE - I_1$$

satisfying an entropy inequality

$$\frac{\partial \mathcal{E}}{\partial t} + \frac{\partial}{\partial x}\big(QE\big) \leq 0.$$

Strict hyperbolicity is lost for $h = 0$, when eigenvectors coincide, representing a so-called "dry state".

2.1 Steady-State Solutions

Smooth steady-state solutions are characterized by two constants, the flow rate Q, and the energy E

$$Q \equiv Au = \text{Const}, \qquad E \equiv \frac{1}{2}u^2 + g(h + B) = \text{Const},$$

of which it is easy to recognize the steady state of rest

$$u = 0, \qquad h + B = \text{Const}.$$

Exact smooth solutions can be found by rootfinding

$$\frac{1}{2}\frac{Q^2}{A^2} + g(h + B) - E = 0, \quad A = A(h). \tag{4}$$

In the straight channel case, smooth steady solutions satisfy (here $h' = h_x$)

$$(F^2 - 1)h' = B'.$$

At the crest $B' = 0$, and the solution is either critical ($F^2 = 1$) or symmetric ($h' = 0$). If the channel is rectangular with variable cross sectional width, then

$$(F^2 - 1)h' = B' - \frac{h\sigma'}{\sigma}F^2. \tag{5}$$

If the crest ($B' = 0$) and the throat ($\sigma' = 0$) occur at the same point, the right hand side of (5) vanishes there and the flow is either symmetric or reaches criticality at that point. Otherwise, criticality occurs where

$$B' = \frac{h}{\sigma}F^2\sigma'$$

which is somewhere between the crest and the throat. For general channels, smooth steady-state solutions satisfy

$$(F^2 - 1)h' = \left(1 - \frac{(\sigma_T - \sigma_B)\ F^2}{\sigma_T}\right)B' - \frac{hI_3}{\sigma_T}F^2.$$

In Appendix A, we discuss further the structure of steady-state solutions and the role of boundary conditions in time dependent problems.

3 Numerical Method

We write system (2) as

$$W_t + A(W)W_x = S(W)$$

and use a Roe-type upwind scheme [21], with upwinding of the geometric source terms as proposed in [22]. The scheme has the general form

$$W_j^{n+1} = W_j^n - \frac{\Delta t}{\Delta x}\left\{A^+_{j-\frac{1}{2}}(W_j^n - W_{j-1}^n) + A^-_{j+\frac{1}{2}}(W_{j+1}^n - W_j^n)\right\}. \tag{6}$$

Here,

$$A^+\Delta W = \sum_{\lambda_k>0}(\alpha_k\lambda_k - \beta_k)r_k, \qquad A^-\Delta W = \sum_{\lambda_k<0}(\alpha_k\lambda_k - \beta_k)r_k \tag{7}$$

where λ_k and r_k are the eigenvalues and eigenvectors of some local linearization of the flux Jacobian, to be specified, and α_k and β_k are the wave strengths associated with the flux gradient and the source

$$\Delta W = \sum_k \alpha_k r_k, \qquad \Delta x S = \sum_k \beta_k r_k \tag{8}$$

given by

$$\begin{aligned}
\alpha_1 &= \frac{(\hat{u}+\hat{c})\Delta A - \Delta Q}{2\hat{c}}, \qquad \beta_1 = \frac{\hat{c}^2(\widehat{\sigma_B}\Delta B - \Delta x\widehat{hI_3}) + \hat{G}}{2\hat{c}} \\
\alpha_2 &= -\frac{(\hat{u}-\hat{c})\Delta A - \Delta Q}{2\hat{c}}, \qquad \beta_2 = -\frac{\hat{c}^2(\widehat{\sigma_B}\Delta B - \Delta x\widehat{hI_3}) + \hat{G}}{2\hat{c}},
\end{aligned} \tag{9}$$

where we have used $\bar{()} = \frac{()_L+()_R}{2}$ to denote arithmetic averages, and $\hat{()}$ to denote other linearized quantities as defined below

$$\begin{aligned}
\hat{A} &= \frac{1}{2}\left[\int_{B_L}^{w_L} + \int_{B_R}^{w_R}\right]\bar{\sigma}(y)dy, \quad \bar{\sigma}(y) = \frac{1}{2}\big(\sigma_L(y) + \sigma_R(y)\big), \\
\hat{u} &= \frac{\sqrt{A_L}u_L + \sqrt{A_R}u_R}{\sqrt{A_L} + \sqrt{A_R}}, \qquad \hat{c}^2 = \frac{g\hat{A}}{\hat{\sigma_T}},
\end{aligned} \tag{10}$$

$\widehat{\sigma_T}$ and $\widehat{\sigma_B}$ are the linearized widths at the top/bottom surface

$$\widehat{\sigma_T}\ \Delta(h+B) = \int_{w_L}^{w_R}\bar{\sigma}(y)dy, \qquad \widehat{\sigma_B}\ \Delta B = \int_{B_L}^{B_R}\bar{\sigma}(y)dy, \tag{11}$$

and

$$\Delta x\widehat{hI_3} = \frac{1}{2}\left[\int_{B_L}^{w_L} + \int_{B_R}^{w_R}\right]\Delta\sigma(y)dy, \qquad \hat{G} = g\int_{w_L}^{w_R}\overline{(w-y)\sigma(x,y)}dy. \tag{12}$$

The above linearization is conservative, and respects steady state of rest (see Appendix B for details), and in the case of vertical walls $\sigma(x, y) = \sigma(x)$, reduces to

$$\hat{A} = \bar{\sigma}\bar{h}, \qquad \widehat{\sigma_T} = \widehat{\sigma_B} = \bar{\sigma} \qquad \hat{c}^2 = g\bar{h}, \qquad \hat{u} = \frac{\sqrt{A_L}u_L + \sqrt{A_R}u_R}{\sqrt{A_L} + \sqrt{A_R}},$$

$$\Delta x \widehat{hI_3} = \bar{h}\ \Delta\sigma, \qquad \hat{G} = \frac{g}{4}\Delta\sigma\,(\Delta(h+B))^2.$$

3.1 A Comment about More General Steady States

The above version of the scheme respects steady state of rest. It is generally not easy to design a scheme that respects *all* steady states, even if smooth, and often necessitates nontrivial rootfinding (see [7, 18, 19]). We would like to make the following observations.

For smooth flows, one may express the governing equations in terms of the equilibrium variables Q and E as follows

$$\begin{aligned} &(A)_t + Q_x = 0, \\ &(Au)_t + uQ_x + AE_x = 0. \end{aligned} \tag{13}$$

This formulation trivially respects *all* smooth steady states, and does not require resorting to rootfinding. Of course, system (13) is not in conservation form, but for smooth flows, computed solutions are conservative to the order of the numerical approximation, which can be as high as one wishes. Where (13) falls short is in handling discontinuous flows.

In [3], a method was proposed for conservation laws with spatially varying flux functions. The method uses the so-called f-waves, and is suitable for computations of near steady-state flows in that the entire residual

$$\Delta F - \Delta x \hat{S}$$

is decomposed onto the characteristic fields, for some linearization of the source $\hat{S}$. If a source linearization can be found so that the steady state is recognized on the discrete level, the residual is identically zero and so are its projections onto the characteristic fields.

For rectangular channels, we write the fluctuations in terms of the equilibrium variables, ΔQ and ΔE. Using repeatedly the identity $\Delta(AB) = \bar{A}\Delta B + \bar{B}\Delta A$ where $\bar{(\cdot)}$ indicates arithmetic average, we obtain

$$\begin{aligned} \Delta\left(\sigma hu^2 + \frac{g}{2}\sigma h^2\right) &\equiv \bar{u}\Delta Q + \overline{\sigma hu}\Delta u + \frac{g}{2}\bar{\sigma}\,\Delta h^2 + \frac{g}{2}\,\overline{h^2}\Delta\sigma \\ &= \bar{u}\Delta Q + \bar{Q}\Delta u + g\bar{\sigma}\ \bar{h}\Delta h + \frac{g}{2}\overline{h^2}\Delta\sigma \\ &= \bar{u}\Delta Q + (\bar{Q} - \bar{\sigma}\ \bar{h}\ \bar{u})\Delta u + \bar{\sigma}\bar{h}\bar{u}\Delta u + g\bar{\sigma}\bar{h}\Delta h + \frac{g}{2}\overline{h^2}\Delta\sigma \\ &= \bar{u}\Delta Q + \bar{\sigma}\bar{h}\Delta\left(\frac{1}{2}u^2 + gh\right) + \frac{g}{2}\overline{h^2}\Delta\sigma + (\bar{Q} - \bar{\sigma}\bar{h}\bar{u})\Delta u. \end{aligned}$$

Using

$$\Delta x\left(\hat{S}\right)^{(2)} = -g\widehat{\sigma h}\Delta B + \frac{1}{2}g\widehat{h^2}\Delta\sigma := -g\bar{\sigma}\bar{h}\Delta B + \frac{1}{2}\,g\overline{h^2}\Delta\sigma$$

we obtain the discrete identity

$$\begin{aligned}\left(\Delta F - \Delta x \bar{S}\right)^{(2)} &= \Delta\left(\sigma h u^2 + \frac{g}{2}\sigma h^2\right) + g\bar{\sigma}\bar{h}\Delta B - \frac{1}{2}g\overline{h^2}\Delta\sigma \\ &= \bar{u}\Delta Q + \bar{\sigma}\bar{h}\Delta E + \underbrace{(\bar{Q} - \bar{\sigma}\bar{h}\bar{u})\Delta u}_{\text{Conservation Correction Term}}.\end{aligned}$$

We make the following comments:

(i) It is easy to see that $\Delta F - \Delta x \bar{S} \equiv 0$ for steady state of rest.

(ii) For more general smooth steady states, $(\Delta F - \Delta x \bar{S})^{(2)} = (\bar{Q} - \bar{\sigma}\bar{h}\bar{u})\Delta u \neq 0$. We observe that

$$\left(\bar{Q} - \bar{\sigma}\bar{h}\bar{u}\right)\Delta u = \left\{\frac{\Delta u \Delta(\sigma h) + \Delta h \Delta(\sigma u) + \Delta\sigma\Delta(hu)}{8}\right\}\Delta u = O(\Delta x)^3$$

is small for smooth flow, so the residual that is being decomposed is very small, which may explain good behavior of the method for general (smooth) steady state.

(iii) The wave strengths expressed in terms of ΔQ and ΔE are given by

$$\begin{aligned}Z_1 &= \frac{1}{2}\Delta Q - \frac{\bar{\sigma}}{2g}\bar{c}\Delta E - \frac{\bar{Q} - \bar{\sigma}\bar{h}\bar{u}}{2\bar{c}}\Delta u, \\ Z_2 &= \frac{1}{2}\Delta Q + \frac{\bar{\sigma}}{2g}\bar{c}\Delta E + \frac{\bar{Q} - \bar{\sigma}\bar{h}\bar{u}}{2\bar{c}}\Delta u.\end{aligned} \tag{14}$$

We have used both versions of the upwind scheme (6)–(12) and (14) in the computations of the next section. In general, we have found them to give very similar results.

3.2 Entropy Fix

It is known that Roe-type schemes require an entropy fix. We have implemented an entropy fix following [11], as discussed in [16]. It is our experience that implementing an entropy fix is crucial for computations of drainage problems, where the flow develops centered rarefactions in regions of very thin layers (see Sect. 4).

3.3 Velocity Regularization and Positivity

When $h \ll 1$ is very small, for example in drainage problems, recovering the velocity u in the standard way $u = Q/A$ becomes inaccurate and may cause instabilities. This is often remedied by regularizing the velocity, for example

$$u = \frac{2Q}{A + \max(A, \epsilon)}. \tag{15}$$

Typically, $\epsilon = O(10^{-5})$. Other formulas may be used [2, 15]. For drainage problems, we have also used

$$u = \text{sign}(Au)\{\max(2(E_{StSt} - g(h + B)), 0)\}^{1/2} \quad \text{for } h < \epsilon \tag{16}$$

which replaces u in very thin layers by a value consistent with the steady-state solution towards which the solution is converging (e.g. E_{StSt} is the final steady-state energy for the drainage problem). This formula often gives very smooth and clean convergence, see numerical results in Sect. 4. The current version of the scheme is not positive, but has proven to be extremely robust in maintaining positivity, for example in drainage problems (see Sect. 4).

4 Numerical Results

The numerical scheme is formulated in terms of integrals over general channel cross section. It is convenient to think of the channel walls as being approximated by straight line segments, leading to piecewise trapezoidal cross sections. In this section, we present results for various shallow flows through channels with various geometries, including rectangular, trapezoidal and general (multi-trapezoidal) cross sectional area. Unless otherwise stated, the examples use $g = 9.81$, a grid of 200 points, and a CFL number of 0.9.

4.1 Rectangular Channels

The examples in this subsection involve channels with rectangular variable (in x) cross sections.

4.1.1 Small Perturbation to Steady State

In the first example, initial data is a small perturbation to steady state of rest. By design, the scheme (6)–(12) preserves steady state of rest, and the propagation of small perturbations thereof is computed very accurately. Computed solutions are shown in Fig. 2, for centered

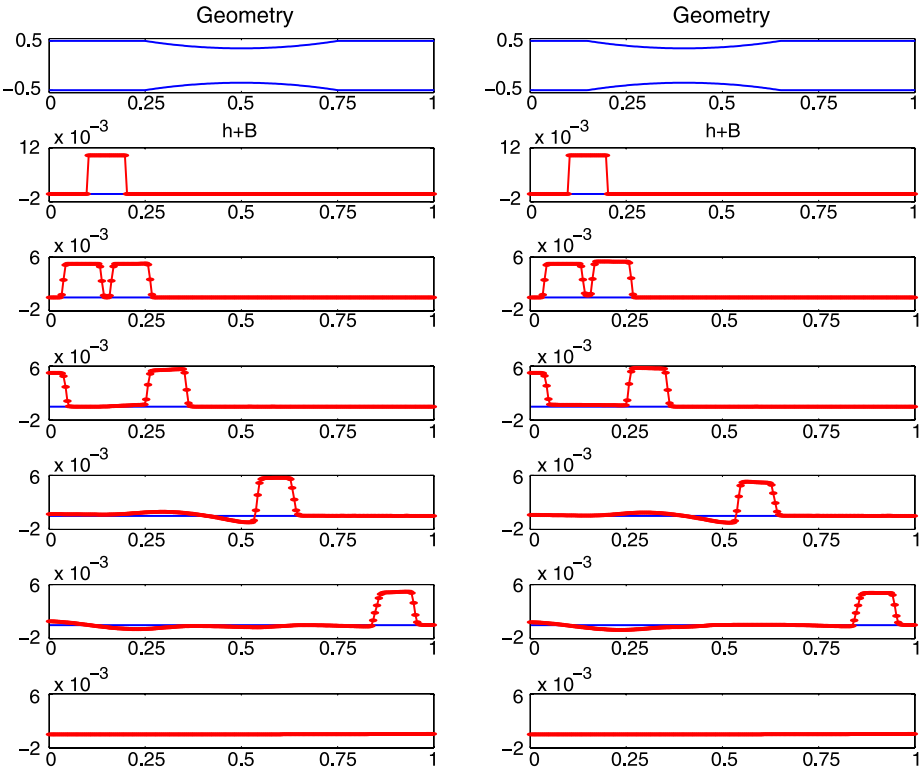

Fig. 2 Propagation of small perturbation to steady state of rest through a contracting rectangular channel, $\epsilon = 10^{-2}$: Centered contraction (*left*) and off centered contraction (*right*), $T = 0$, 0.02, 0.05, 0.15, 0.25 and 0.5

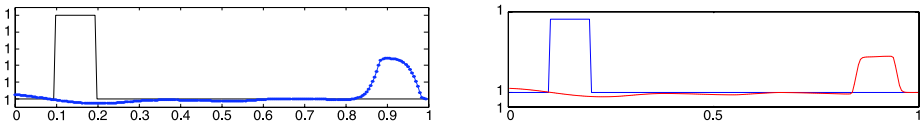

Fig. 3 Propagation of small disturbance to steady state of rest through a contracting rectangular channel, $\epsilon = 10^{-5}$. Total water height, $w = h + B$, at $t = 0.25$ (*dots*) over initial conditions (*solid line*): central-upwind [2] (*left*) and upwind (*right*) schemes

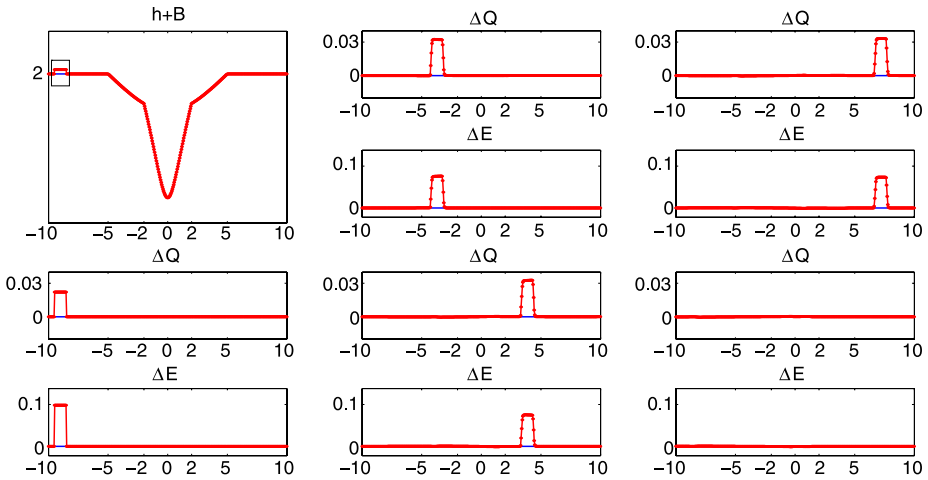

Fig. 4 Propagation of small perturbation to non-rest steady state through a contracting rectangular channel, $\epsilon = 10^{-2}$, centered contraction. The total height for the initial perturbation (*top left*) and the equilibrium variables for $T = 0$, 0.8, 1.9, 2.4 and 4 are shown

and off-centered channel contractions. Once the small perturbation leaves the computational domain, the unperturbed steady state is recovered.

A comparison with results by the central-upwind scheme [2] are shown in Fig. 3 for $\epsilon = 10^{-5}$, on a grid of 200 points. Results are similar, with the upwind scheme better able to maintain a sharp profile of the perturbation.

The propagation of a small perturbation to a non-rest steady state is shown in Fig. 4. Again, once the perturbation leaves the computational domain, the unperturbed steady state is recovered, indicated by Q and E going back to their constant unperturbed levels.

4.1.2 Convergence to Steady State

The next set of examples illustrates the long time convergence of transient solutions to a steady state. The channel has vertical walls, with a parabolic contraction. In all cases, the flow discharge Q was imposed at inflow, and the depth of the layer h was imposed at (subcritical) outflow. Figure 5 (top) shows a schematic of the geometry (not drawn to scale) and includes a straight channel, a channel with centered contraction and a channel with off-centered contraction. Below the geometry, Fig. 5 shows the topography B and water level $h + B$ at steady state for (i) subcritical flow (top middle), (ii) smooth transcritical flow (bottom middle) and (iii) transcritical flow with a jump (bottom). The following boundary conditions were specified for (i) straight channel (ii) centered and (iii) off-centered contraction

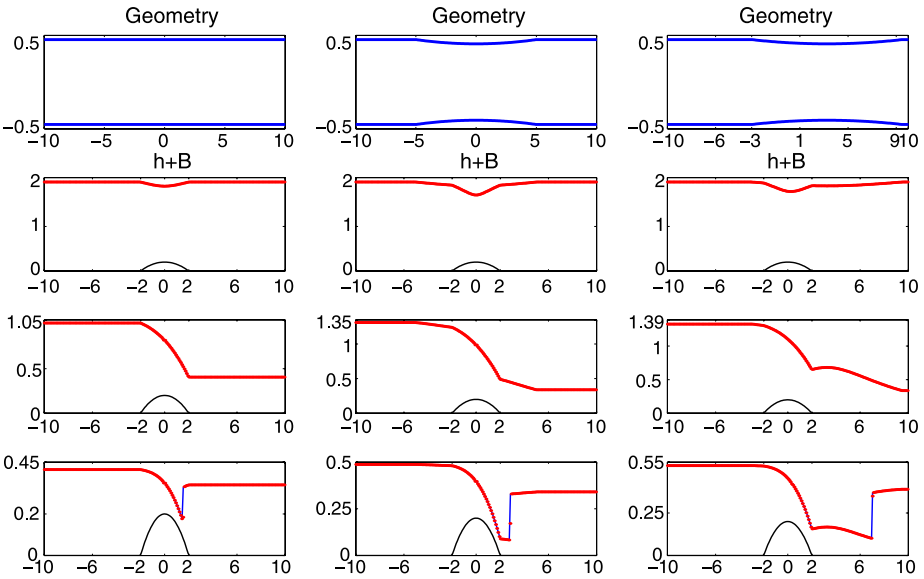

Fig. 5 Numerical (*symbol*) and exact (*solid line*) water level in steady-state solutions: Geometry (*top*), subcritical flow (*top middle*), smooth transcritical flow (*bottom middle*) and transcritical flow with a jump (*bottom*); Rectangular channel with straight walls (*left*), centered contraction (*middle*) and off-center contraction (*right*)

Table 1

	Q_{in}	h_{out}	$\sigma_{\min}$	x_0	x_1	
subcritical flow:	4.42	2.0	1.0	−10	10	: straight
			0.9	−5	5	: centered
			0.9	−3	9.5	: off-centered
smooth transcritical flow:	1.53	0.4058	1.0	−10	10	: straight
		0.3384	0.7	−5	5	: centered
		0.3356	0.6	−3	9.5	: off-centered
transcritical flow with jump:	0.18	0.34	1.0	−10	10	: straight
		0.34	0.66	−5	5	: centered
		0.39	0.4	−3	9.5	: off-centered

respectively. The bottom topography in all the examples is $B(x) = \max\{(0.05(4 - x^2), 0)\}$. The geometry is given by a parabolic contraction extending from x_0 to x_1, as specified in Table 1. Computed solutions are in excellent agreement with exact solutions, also shown.

Figure 6 shows a comparison between the present upwind scheme and the central scheme of [2]. The examples were taken from [2]. See Fig. 9 (bottom), Fig. 10 (top) and Fig. 11 (bottom) therein. By design, both schemes respect steady state of rest, but neither is able to preserve general steady states. The closeness of Q and E to being constants is a good measure of how well the schemes do in approximating general (smooth) steady states. It is

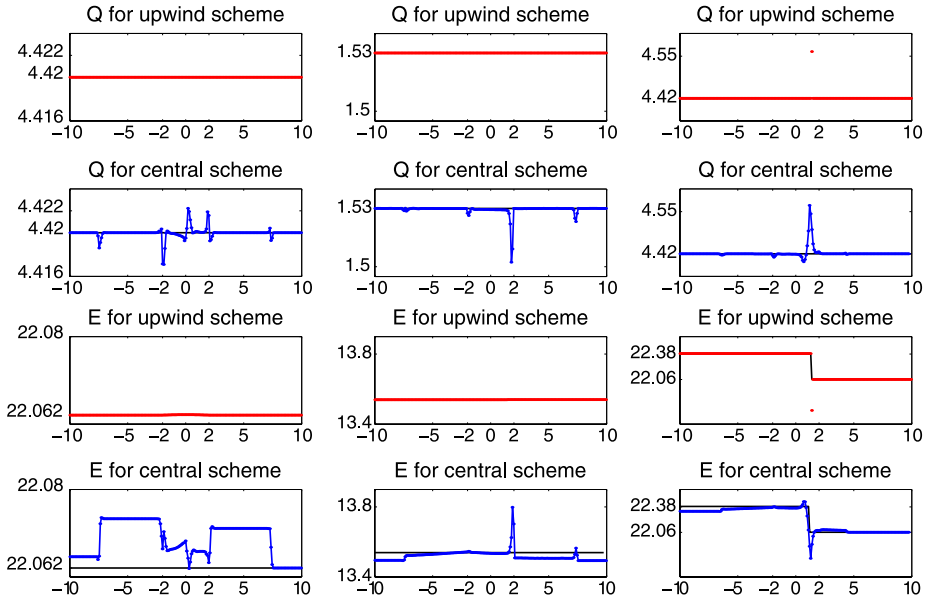

Fig. 6 Comparison between the upwind and the central schemes for convergence to steady states. For channels with vertical walls, equilibrium variables Q and E are shown for a subcritical (*left*), smooth transcritical (*middle*), and discontinuous transcritical (*right*) flow

striking to note that the present upwind scheme converges to Q and E with relative errors consistently 2–4 orders of magnitude better than the central-upwind scheme.

4.1.3 Reservoir Drainage after Dam Break

In the next example, a reservoir is being drained through a contracting channel. The water is initially at rest $u = 0$, leveled at $h + B = 0.8$. The water drains through the right boundary, the left boundary is assumed a line of symmetry of the domain and wall boundary conditions are applied, trapping the water to the left of the bump. Computed solution is shown in Fig. 7 for various intermediate times, the reservoir has essentially drained by $T = 15$. The equilibrium variables Q and E are also shown for the solution at the final time.

Figure 8 compares the computed solution using the velocity regularization (15) and (16) respectively. It can be observed that the regularization (15) results in a more noisy drained solution, while regularization (16), which makes use of the steady-state energy E_{StSt} in the trough converges to a cleaner and generally more accurate solution.

Figure 9 shows reservoir drainage through a contracting channel, this time over a double bump topography. The water now gets trapped in two troughs. Despite the fact that the scheme is not positive, the computed solution remains positive and we are able to integrate this solution for very long time until drainage is reached. The equilibrium variables Q and E corresponding to the final time are also shown.

4.2 More General Channels

The following tests involve channels of general cross section described by $\sigma(x, y)$. We present examples for channels consisting of one, two or several trapezoids. Exact solutions

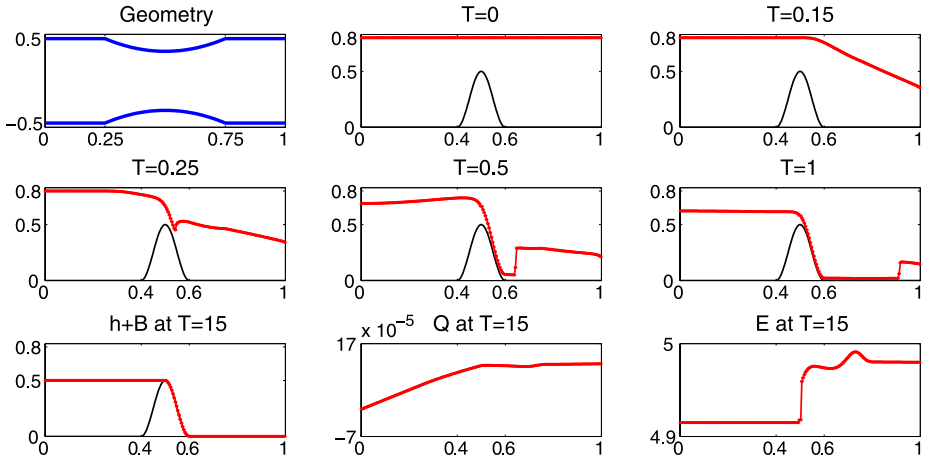

Fig. 7 Reservoir drainage after dam break. The equilibrium variables at $T = 15$ are also shown

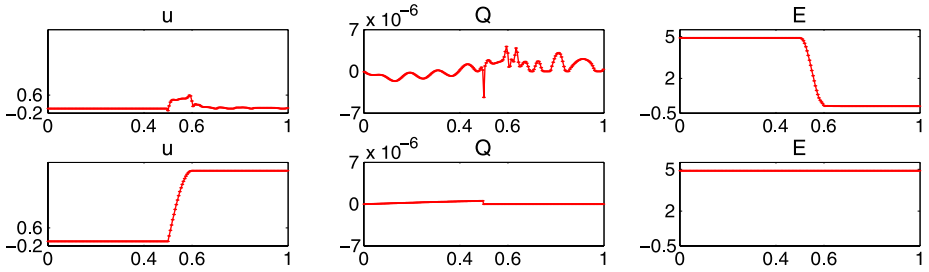

Fig. 8 Reservoir drainage after dam break. Comparison at $T = 50$ of the computed velocity and equilibrium variables using regularization (15) (*top*) and regularization (16) (*bottom*)

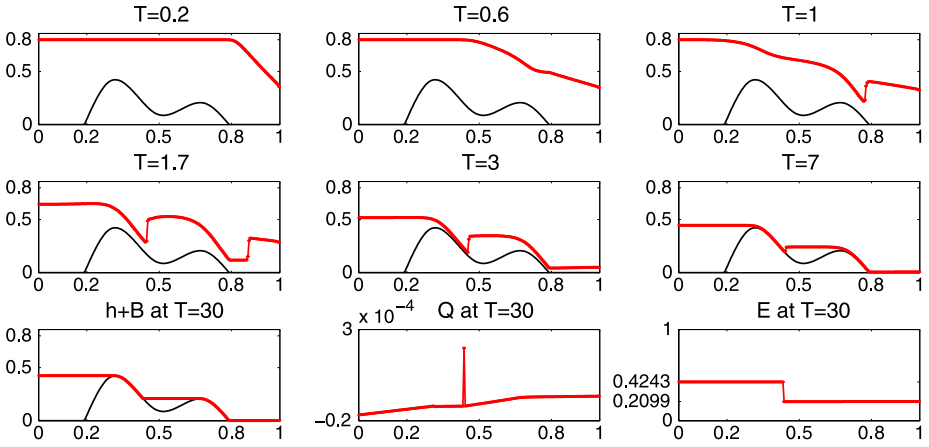

Fig. 9 Reservoir drainage after dam break. The equilibrium variables are also shown for $T = 30$

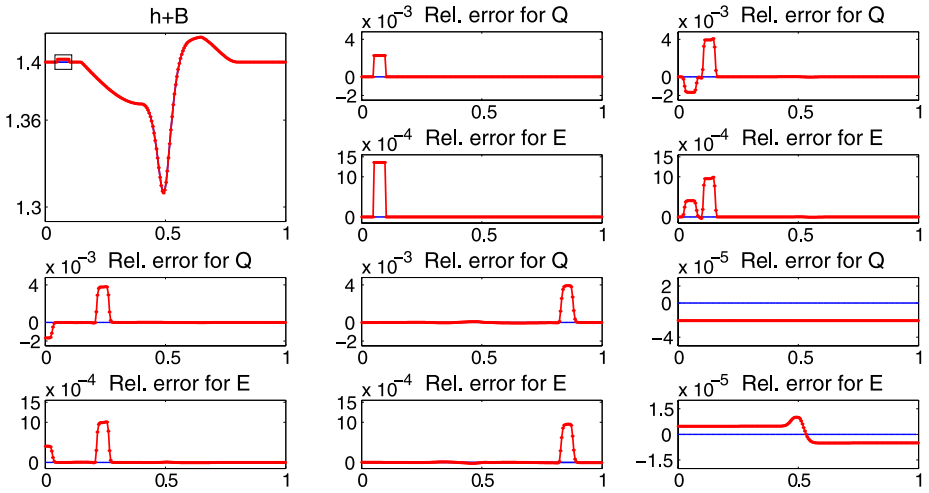

Fig. 10 Small perturbation to steady state of non-rest for a trapezoidal channel, $\epsilon = 2 \times 10^{-3}$, non-centered contraction. The total height for the initial perturbation (*top left*) and the relative errors for the equilibrium variables for $T = 0$, 0.014, 0.04, 0.19, and 20 are shown

are also computed and are compared to computations. We use $\chi_{[a,b]}(x)$ to denote the characteristic function of the interval $[a, b]$.

4.2.1 Propagation of Small Perturbation to Non-Rest Steady State

In this test, the topography is a cosine bump $B(x) = \chi_{[0.4,0.6]}(x)\frac{1}{4}(\cos(\pi(x-1/2)/0.1)+1)$. The channel has a trapezoidal cross section with variable (in x) wall inclination $\sigma(x, y) = \sigma_B(x) + m(x)y$, with $m(x) = 2 + \chi_{[0.4,0.8]}(x)\frac{1}{4}(\cos(\pi(x - 0.6)/0.2) + 1)$, and $\sigma_B(x) = \min(1, 0.7 + 4.8(x - 0.4)^2)$. In this example, the steady-state flow is subcritical, with $Q = 4$ and $h_{out} = 1.4$. The size of the perturbation is $\epsilon = 2 \times 10^{-3}$. The initial disturbance to the interface, as well as the relative errors for the equilibrium variables are shown in Fig. 10. We observe that the unperturbed steady state is recovered very accurately.

4.2.2 Convergence to Steady States for Trapezoidal Channel

We next study the convergence of transient solutions to steady state. The topography and geometry are the same as in the previous test. For subcritical flow, $Q = 4.42$ and $h_{out} = 1.47$. For smooth transcritical flow, $Q = 8.4992$ and $h_{out} = 1.0388$. For discontinuous transcritical flow, $Q = 1.1104$ and $h_{out} = 0.7195$. Computed and exact solutions are shown in Fig. 11, with very good agreement.

4.2.3 Convergence to Steady States for Piecewise Trapezoidal Channel

In this test, each cross section of the channel consists of two trapezoid, with variable (in x) wall inclination. The bottom trapezoid, with height $y = 1.2$, is the same as in the previous example, and the wall of the top trapezoid has twice the slope of the bottom one. Convergence of transient solutions to steady state are shown in Fig. 12 for subcritical (left), smooth transcritical (middle) and discontinuous (right) flows. Agreement between computed and exact solutions is excellent.

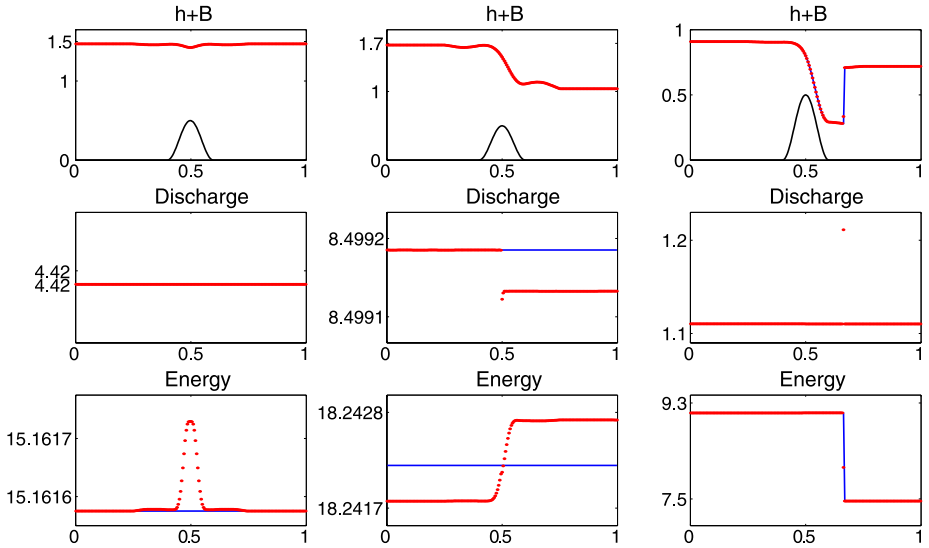

Fig. 11 Numerical (*symbol*) and exact (*solid line*) solutions in steady-state flows: Water level (*top*), discharge (*middle*) and energy (*bottom*); Subcritical flow (*left*), smooth transcritical flow (*middle*) and transcritical flow with a jump (*right*)

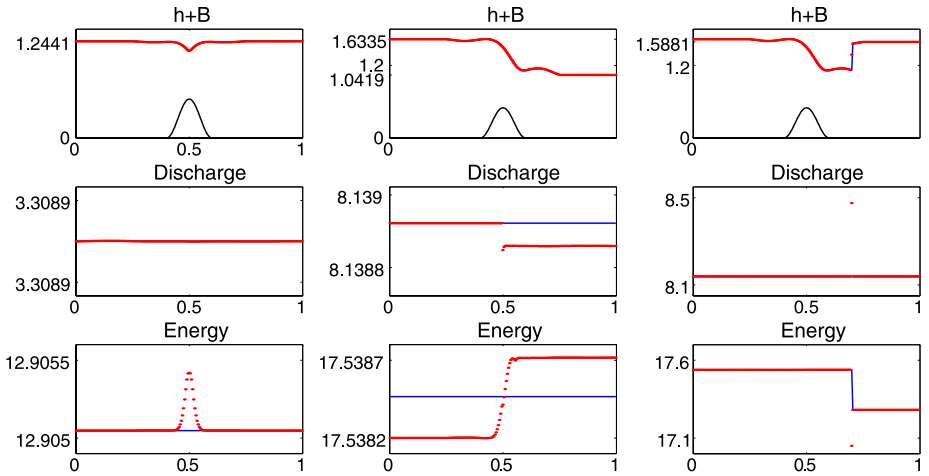

Fig. 12 Convergence to steady state for a trapezoidal channel (two trapezoids). Total height (*top*), discharge (*middle*), and energy (*bottom*) are shown for subcritical (*left*), smooth transcritical (*center*) and discontinuous transcritical (*right*) flows

4.3 Convergence to Steady State for General Channels

The last example concerns flow in a channel whose geometry is given by

$$\sigma(x,y) = 1 + \frac{3}{4}\cos(\pi x) - \frac{1}{4}\chi_{[0.4,0.6]}(x)(\cos(\pi(x-1/2)/0.1)+1) + \sqrt{y}\left(1 - \frac{1}{4}\chi_{[0.1,0.7]}(x)(\cos(\pi(x-0.4)/0.3)+1)\right)$$

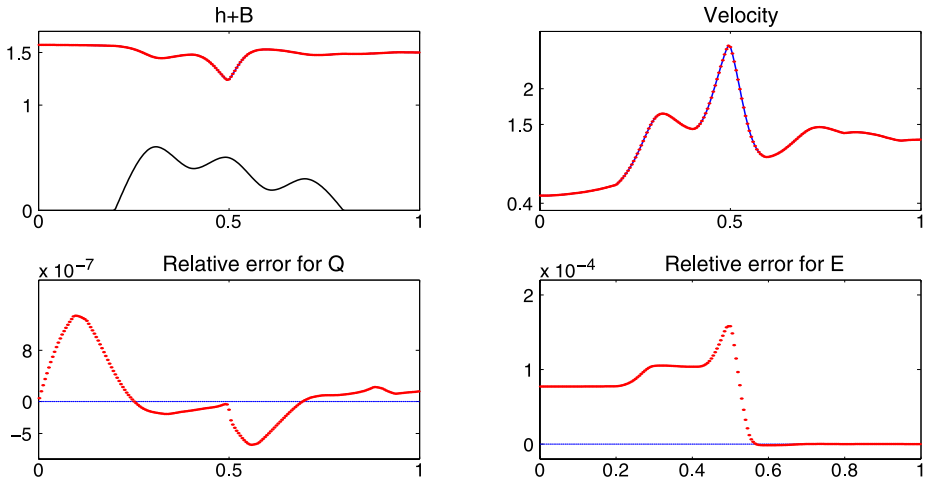

Fig. 13 Convergence to a subcritical flow. Exact and numerical solutions are plotted with excellent agreement. The top surface, topography (*top left*), velocity (*top right*), and relative errors for the equilibrium variables (*bottom*) are shown

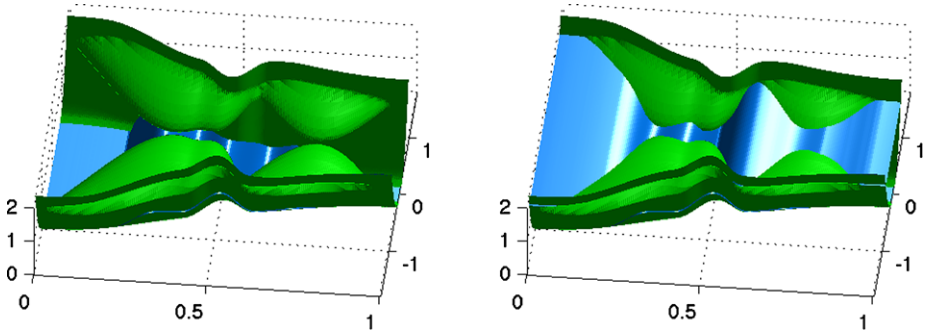

Fig. 14 3D view of the channel (*left*) and the channels with the subcritical flow (*right*) given in Fig. 13

$$-2\chi_{[0,1]}\left(\frac{(x-0.3)^2+(y-1.4)^2}{r_1^2}\right)\cos\left(\sqrt{\frac{(x-0.3)^2+(y-1.4)^2}{r_1^2}}\frac{\pi}{2}\right)$$

$$-1.6\chi_{[0,1]}\left(\frac{(x-0.75)^2+(y-1.4)^2}{r_2^2}\right)\cos\left(\sqrt{\frac{(x-0.75)^2+(y-1.4)^2}{r_1^2}}\frac{\pi}{2}\right),$$

where $r_1 = 0.28$, $r_2 = 0.2$. The topography is a 3-bump spline with nodes $(x, y) = (0.2, 0)$, $(0.3, 0.6)$, $(0.4, 0.4)$, $(0.5, 0.5)$, $(0.6, 0.2)$, $(0.7, 0.3)$ and $(0.8, 0)$, shown on top left of Fig. 13. In this example $Q = 2.0583$ and $h_{out} = 1.5$. The cross section is approximated by 50 trapezoids. The results in Fig. 13 show excellent agreement between the computed and exact steady-state solutions. The relative errors for the equilibrium variables Q and E are of orders 10^{-6} and 10^{-4} respectively. Figure 14 shows a 3D view of the flow.

Acknowledgements The authors would like to thank Alfredo Wetzel for his help with computing exact steady-state solutions, and Jorge Balbás for helpful discussions and for providing data for comparisons be-

tween central and upwind schemes. Part of this work was done while Gerardo Hernández-Dueñas was visiting IPAM at UCLA. The hospitality of the program organizers is gratefully acknowledged.

Appendix A: Steady States and Boundary Conditions

The structure of steady-state solutions plays a role in specifying boundary conditions in time dependent problems. We consider the straight channel case, $\sigma = 1$, and assume that Q and E are specified. At a given elevation $B(x)$, h can be found from (4) by rootfinding. Is easy to compute $B(h)$ and reverse their roles to plot $h(B)$, see Fig. 15. We observe that only values of B below some B^* can be supported for given Q and E. Within that range, for any given value of B, there are two possible values of h, corresponding to subcritical flow (top branch) and to supercritical flow (bottom branch). At B^*, one has $B'(h) = 0$, which can be easily shown to imply $F^2 = u^2/(gh) = 1$, that is the flow is critical at B^*.

Consider a flow from left to right over a bump in B that vanishes near the domain boundaries. A solution that starts off as subcritical at inflow, accelerates as the flow runs over the bump, and its Froude number increases. The solution moves to the right along the top subcritical branch of the curve, until it reaches the crest at some $B_{\max} < B^*$, beyond which the flow starts decelerating, its Froude number decreases, and the solution moves back along the top subcritical branch, to meet the boundary condition at outflow. For the case $B_{\max} = B^*$, the solution moves along the subcritical branch all the way to B^*, becomes critical and 'turns' around to the supercritical branch. It then continues along the supercritical branch, its Froude number continues to increase, to meet the boundary condition at outflow. This flow accelerates smoothly from sub- to supercritical flow (similar to Laval nozzle flow in converging-diverging channels). In reference to Fig. 15, h_1 and h_2 are the only boundary conditions at outflow that produce smooth solutions: h_1 produces a symmetric subcritical flow, and h_2 an asymmetric transcritical flow. To adjust to any other boundary condition at outflow the flow must form a discontinuity. Figure 15 (right) shows several curves of h vs. B for the same Q but different values of E. Each one of those curves corresponds to a different smooth steady solution. A flow that starts off as subcritical at inflow along the red curve, and needs to adjust to h_3 at outflow, becomes critical as it reaches $B_{\max}$ then supercritical along the bottom red branch. It then jumps from the red curve to the top (subcritical) branch of the dashed green curve, a curve that corresponds to a (lower) value of E, and continues smoothly along this branch to meet the outflow boundary condition. The jump between curves occurs at the point where the shock jump conditions are satisfied. Symmetric and asymmetric transcritical solutions are illustrated in Fig. 16.

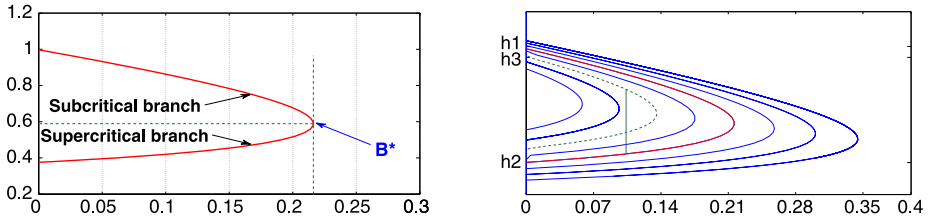

Fig. 15 Smooth (*left*) and discontinuous (*right*) steady-state solutions, h vs. B

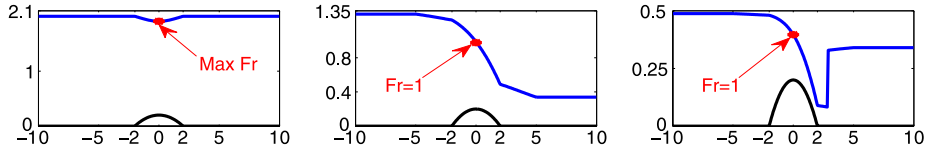

Fig. 16 Steady flow in a channel: Symmetric subcritical (*left*); Asymmetric transcritical (*middle*); and Asymmetric transcritical with a shock (*right*)

Appendix B: Derivation of the Linearization

B.1 Conservation

We consider system (1), and relate the conservative and quasilinear forms. At the differential level we have

$$\begin{pmatrix} Au \\ Au^2 + I_1 \end{pmatrix}_x = \begin{pmatrix} 0 & 1 \\ c^2 - u^2 & 2u \end{pmatrix} \begin{pmatrix} A \\ Au \end{pmatrix}_x + \begin{pmatrix} 0 \\ c^2(-hI_3 + \sigma_B B_x) + \underline{I_2 - g\sigma_B h B_x} \end{pmatrix}, \quad (17)$$

where the geometric terms on the right hand side arise from careful application of the Fundamental Theorem of Calculus (FTC) to I_1. We further note that the underlined geometric term in (17) cancels out with an identical term in the geometric source in (1), and while it appears in the derivation of the method, it 'washes out' and ends up not playing a role in the method. We focus on the second component of this vector equation, and seek a discrete analogue. We use the following discrete version of the FTC

$$\begin{aligned} \Delta \int_{a(x)}^{b(x)} f(y,x)dy &\equiv \int_{a_R}^{b_R} f(y,x_R)dy - \int_{a_L}^{b_L} f(y,x_L)dy \\ &= \frac{1}{2}\left(\int_{a_L}^{b_L} + \int_{a_R}^{b_R}\right)\Delta f(y)dy + \int_{b_L}^{b_R} \bar{f}(y)dy - \int_{a_L}^{a_R} \bar{f}(y)dy, \end{aligned} \quad (18)$$

where we have used here and in what follows $\Delta(\,) = (\,)_R - (\,)_L$, and $\overline{(\,)} = ((\,)_R + (\,)_L)/2$.

The discrete version of (17) requires the flux difference $\Delta(Au^2 + I_1)$. We begin by seeking a linearization of $\hat{u}$ for which

$$\Delta(Au^2) = 2\hat{u}\Delta(Au) - \hat{u}^2\Delta A$$

which is satisfied by the familiar expression

$$\hat{u} = \frac{\sqrt{A_L}u_L + \sqrt{A_R}u_R}{\sqrt{A_L} + \sqrt{A_R}}.$$

We next apply the discrete FTC (18) to express ΔI_1

$$\begin{aligned} \Delta I_1 &= g\Delta \int_B^w (w-y)\sigma(x,y)dy \\ &= \frac{g}{2}\left[\int_{B_L}^{w_L} + \int_{B_R}^{w_R}\right]\Delta\big((w-y)\sigma(x,y)\big)dy + g\int_{w_L}^{w_R} \overline{(w-y)\sigma(x,y)}dy \\ &\quad - g\int_{B_L}^{B_R} \overline{(w-y)\sigma(x,y)}dy \end{aligned}$$

$$= \frac{g}{2}\left[\int_{B_L}^{w_L} + \int_{B_R}^{w_R}\right](\bar{\sigma}(y)\Delta w + (\bar{w} - y)\Delta\sigma(y))dy + g\int_{w_L}^{w_R}\overline{(w-y)\sigma(x,y)}dy$$
$$- g\int_{B_L}^{B_R}\overline{(w-y)\sigma(x,y)}dy$$
$$= g\hat{A}\Delta w + \Delta x\ \hat{I}_2 + \hat{G} - g\widehat{\sigma_B h}\Delta B \tag{19}$$

where we define

$$\hat{A} := \frac{1}{2}\left[\int_{B_L}^{w_L} + \int_{B_R}^{w_R}\right]\bar{\sigma}(y)dy, \qquad \Delta x\widehat{I_2} := \frac{g}{2}\left[\int_{B_L}^{w_L} + \int_{B_R}^{w_R}\right](\bar{w} - y)\Delta\sigma(y)dy,$$
$$\hat{G} := g\int_{w_L}^{w_R}\overline{(w-y)\sigma(x,y)}dy, \qquad g\widehat{\sigma_B h}\Delta B := g\int_{B_L}^{B_R}\overline{(w-y)\sigma(x,y)}dy.$$

In order to express Δw in (19) in terms of the conserved variables, we apply the discrete FTC (18) to the wet area $A(x) = \int_B^w \sigma(x, y)dy$ and obtain

$$\Delta A = \frac{1}{2}\left[\int_{B_L}^{w_L} + \int_{B_R}^{w_R}\right]\Delta\sigma(y)dy + \int_{w_L}^{w_R}\bar{\sigma}(y)dy - \int_{B_L}^{B_R}\bar{\sigma}(y)dy$$
$$= \Delta x\widehat{hI_3} + \widehat{\sigma_T}\Delta(h+B) - \widehat{\sigma_B}\Delta B, \tag{20}$$

where we define

$$\Delta x\widehat{hI_3} := \frac{1}{2}\left[\int_{B_L}^{w_L} + \int_{B_R}^{w_R}\right]\Delta\sigma(y)dy, \qquad \widehat{\sigma_T}\ \Delta(h+B) := \int_{w_L}^{w_R}\bar{\sigma}(y)dy,$$
$$\widehat{\sigma_B}\ \Delta B := \int_{B_L}^{B_R}\bar{\sigma}(y)dy.$$

Rearranging (20) yields

$$\Delta(h+B) = \frac{1}{\widehat{\sigma_T}}\left\{\Delta A + \hat{\sigma_B}\Delta B - \Delta x\widehat{hI_3}\right\} \tag{21}$$

and ΔI_1 becomes

$$\Delta I_1 = \frac{g\hat{A}}{\widehat{\sigma_T}}\left[\Delta A + \widehat{\sigma_B}\Delta B - \Delta x\widehat{hI_3}\right] + \hat{G} + \Delta x\widehat{I_2} - g\widehat{\sigma_B h}\Delta B.$$

This suggest to define

$$\hat{c}^2 = \frac{g\hat{A}}{\widehat{\sigma_T}}$$

yielding

$$\Delta I_1 = \hat{c}^2\Delta A + \hat{c}^2[-\Delta x\widehat{hI_3} + \widehat{\sigma_B}\Delta B] + \hat{G} + \Delta x\ \hat{I}_2 - g\widehat{\sigma_B h}\Delta B.$$

The discrete version of (17) then becomes

$$\Delta\begin{pmatrix} Au \\ Au^2 + I_1 \end{pmatrix} = \begin{pmatrix} 0 & 1 \\ \hat{c}^2 - \hat{u}^2 & 2\hat{u} \end{pmatrix}\begin{pmatrix} \Delta A \\ \Delta(Au) \end{pmatrix} + \begin{pmatrix} 0 \\ \hat{c}^2(-\Delta x\widehat{hI_3} + \widehat{\sigma_B}\,\Delta B) + \hat{G} + \Delta x\widehat{I_2} - g\widehat{\sigma_B h}\,\Delta B \end{pmatrix}, \tag{22}$$

and the last two terms cancel out with identical terms in the numerical approximation of the geometric source, in the same way that they do at the differential equation level in (1).

It is easy to verify that

$$\Delta\begin{pmatrix} Au \\ Au^2 + I_1 \end{pmatrix} - \Delta x\begin{pmatrix} 0 \\ \Delta x\widehat{I_2} - g\widehat{\sigma_B h}\Delta B \end{pmatrix} = \sum_k (\lambda_k\alpha_k - \beta_k)r_k$$

where

$$\alpha_1 = \frac{(\hat{u}+\hat{c})\Delta A - \Delta(Au)}{2\hat{c}}, \qquad \beta_1 = \frac{\hat{c}^2(\widehat{\sigma_B}\Delta B - \Delta x\widehat{hI_3}) + \hat{G}}{2\hat{c}},$$
$$\alpha_2 = -\frac{(\hat{u}-\hat{c})\Delta A - \Delta(Au)}{2\hat{c}}, \qquad \beta_2 = -\frac{\hat{c}^2(\widehat{\sigma_B}\Delta B - \Delta x\widehat{hI_3}) + \hat{G}}{2\hat{c}}.$$

B.2 Respecting Steady State of Rest

Consider the total fluctuation in the first wave family

$$\alpha_1\lambda_1 - \beta_1 = (\hat{u}-\hat{c})\frac{(\hat{u}+\hat{c})\Delta A - \Delta(Au)}{2\hat{c}} - \frac{\hat{c}^2(\widehat{\sigma_B}\Delta B - \Delta x\widehat{hI_3}) + \hat{G}}{2\hat{c}}$$

which, for steady state of rest, $u = 0,\ \Delta(h+B) = 0$, reduces to

$$\alpha_1\lambda_1 - \beta_1 = -\frac{\hat{c}}{2}\left(\Delta A + \widehat{\sigma_B}\Delta B - \Delta x\widehat{hI_3}\right) = -(\alpha_2\lambda_2 - \beta_2)$$

and observe that (21) implies the total fluctuation vanishes, which insures that steady states of rest are recognized and respected.

References

1. Audusse, E., Bouchut, F., Bristeau, M.O., Klein, R., Perthame, B.: A fast and stable well-balanced scheme with hydrostatic reconstruction for shallow water flows. SIAM J. Sci. Comput. **25**, 2050–2065 (2004)
2. Balbás, J., Karni, S.: A central scheme for shallow water flows along channels with irregular geometry. ESAIM: Math. Model. Numer. Anal. **43**, 333–351 (2009)
3. Bale, D.S., LeVeque, R.J., Mitran, S., Rossmanith, J.A.: A wave propagation method for conservation laws and balance laws with spatially varying flux functions. SIAM J. Sci. Comput. **24**(3), 955–978 (2002)
4. Bouchut, F.: Nonlinear Stability of Finite Volume Methods for Hyperbolic Conservation Laws and Well-Balanced Schemes for Sources. Frontiers in Mathematics. Birkhäuser, Basel (2004)
5. Castro, M.J., Macias, J., Pares, C.: A Q-scheme for a class of systems of coupled conservation laws with source terms. Application to a two-layer 1-d shallow water system. ESIAM: M2AN **35**, 107–127 (2001)
6. Castro, M.J., García-Rodríguez, J.A., González-Vida, J.M., Macías, J., Parés, C., Vázquez-Cendón, M.E.: Numerical simulation of two-layer shallow water flows through channels with irregular geometry. J. Comput. Phys. **195**, 202–235 (2004)

7. Castro, M.J., Pardo Milanés, A., Parés, C.: Well-balanced numerical schemes based on a generalized hydrostatic reconstruction technique. Math. Models Methods Appl. Sci. **17**(12), 2055–2113 (2007)
8. Črnjarić-Žic, N., Vuković, S., Sopta, L.: Balanced finite volume WENO and central WENO schemes for the shallow water and the open-channel flow equations. J. Comput. Phys. **200**, 512–548 (2004)
9. Garcia-Navarro, P., Vazquez-Cendon, M.E.: On numerical treatment of source terms in the shallow water equations. Comput. Fluids **29**, 951–979 (2000)
10. George, D.L.: Augmented Riemann solvers for the shallow water equations over variable topography with steady states and inundation. J. Comput. Phys. **227**, 3089–3113 (2008)
11. Harten, A., Hyman, J.M.: Self adjusting grid methods for one-dimensional hyperbolic conservation laws. J. Comput. Phys. **50**, 235–269 (1983)
12. Jin, S.: A steady-state capturing method for hyperbolic systems with geometrical source terms. ESIAM: Math. Model. Numer. Anal. **35**(4), 631–645 (2001)
13. Karni, S., Hernández-Dueñas, G.: A scheme for the shallow water flow with area variation. In: International Conference on Numerical Analysis and Applied Mathematics, Rethymno, Crete, Greece. AIP Conference Proceedings, vol. 1168, pp. 1433–1436. American Institute of Physics, New York (2009)
14. Kurganov, A., Levy, D.: Central-upwind schemes for the Saint-Venant system. ESIAM: Math. Model. Numer. Anal. **36**(3), 397–425 (2002)
15. Kurganov, A., Petrova, G.: A second-order well-balanced positivity preserving central-upwind scheme for the Saint-Venant system. Commun. Math. Sci. **5**(1), 133–160 (2007)
16. LeVeque, R.J.: Numerical Methods for Conservation Laws, 2nd edn. Birkhäuser, Basel (1992)
17. LeVeque, R.J.: Balancing source terms and flux gradients in high-resolution Gudonov methods: the quasi-steady wave-propagation algorithm. J. Comput. Phys. **146**, 346–365 (1998)
18. Noelle, S., Pankratz, N., Puppo, G., Natvig, J.R.: Well-balanced finite volume schemes of arbitrary order of accuracy for shallow water flows. J. Comput. Phys. **213**, 474–499 (2006)
19. Noelle, S., Xing, Y., Shu, C.-W.: High-order well-balanced finite volume WENO schemes for shallow water equation with moving water. J. Comput. Phys. **226**, 29–58 (2007)
20. Perthame, B., Simeoni, C.: A kinetic scheme for the Saint-Venant system with a source term. Calcolo **38**(4), 201–231 (2001)
21. Roe, P.L.: Approximate Riemann solvers, parameter vectors, and difference schemes. J. Comput. Phys. **43**, 357–372 (1981)
22. Roe, P.L.: Upwind differencing schemes for hyperbolic conservation laws with source terms. In: Nonlinear Hyperbolic Problems. Proc. Adv. Res. Workshop, St. Étienne, 1986. Lect. Notes Math., vol. 1270, pp. 41–51. Springer, Berlin (1987)
23. Russo, G.: Central schemes for balance laws. In: Hyperbolic Problems: Theory, Numerics, Applications, vols. I, II, Magdeburg, 2000. Internat. Ser. Numer. Math., vol. 140, pp. 821–829. Birkhäuser, Basel (2001)
24. Vázquez-Cendón, M.E.: Improved treatment of source terms in upwind schemes for the shallow water equations in channels with irregular geometry. J. Comput. Phys. **148**, 497–526 (1999)
25. Vukovič, S., Sopta, L.: High-order ENO and WENO schemes with flux gradient and source term balancing. In: Applied Mathematics and Scientific Computing, Dubrovnik, 2001, pp. 333–346. Kluwer/Plenum, New York (2003)